



# Removal of sulfadiazine from aqueous solution by magnetic biochar prepared with pomegranate peel

Tülay Oymak & Elif Sena Şafak


To cite this article: Tülay Oymak & Elif Sena Şafak (2022) Removal of sulfadiazine from aqueous solution by magnetic biochar prepared with pomegranate peel, Separation Science and Technology, 57:16, 2521-2531, DOI: [10.1080/01496395.2022.2081205](https://doi.org/10.1080/01496395.2022.2081205)


To link to this article: <https://doi.org/10.1080/01496395.2022.2081205>

 View supplementary material [↗](#)

 Published online: 31 May 2022.

 Submit your article to this journal [↗](#)

 Article views: 74

 View related articles [↗](#)

 View Crossmark data [↗](#)



## Removal of sulfadiazine from aqueous solution by magnetic biochar prepared with pomegranate peel

Tülay Oymak and Elif Sena Şafak

Faculty of Pharmacy, Department of Analytical Chemistry, Sivas Cumhuriyet University, Turkey

### ABSTRACT

Magnetic biochar ( $\text{Fe}_3\text{O}_4$ -BCPP) was prepared by using iron oxide nanoparticles, and biochar which is obtained from pomegranate peel. The  $\text{Fe}_3\text{O}_4$ -BCPP were characterized by Brunauer-Emmett-Teller analysis, X-ray diffraction analysis, scanning electron microscopy, and vibrating sample magnetometer. The adsorption properties of  $\text{Fe}_3\text{O}_4$ -BCPP for sulfadiazine in water were investigated. The  $\text{Fe}_3\text{O}_4$ -BCPP had good adsorption properties and separated well from aqueous solution by a permanent magnet due to superparamagnetic property and magnetic saturation value. Therefore,  $\text{Fe}_3\text{O}_4$ -BCPP has potential application for the removal of sulfadiazine from water samples.

### ARTICLE HISTORY

Received 1 November 2021  
Accepted 17 May 2022

### KEYWORDS

Magnetic biochar;  
pomegranate peel;  
sulfadiazine; adsorption

### Introduction

Antibiotics are an important class of pharmaceuticals which are widely used in humans and animals to prevent or treat infectious diseases caused by pathological micro-organisms. A large proportion of antibiotics are partially metabolized in organisms and the main components or metabolites are excreted through urine and feces. However, antibiotics from local authority waste water treatment systems and from pharmaceutical production facilities are mixed with the natural water reserves. Pharmaceutical chemicals, especially antibiotics, are classified as uncontrollable bioaccumulative components. Studies in recent years have determined antibiotic residue in different environments such as waste water treatment facilities, hospitals, subterranean water, and livestock farms.<sup>[1,2]</sup> Despite the low concentration range of antibiotics in water, they can remain for a long time without decomposing and cause changes in the microbial ecology, increase productivity of antibiotic-resistant pathogens and cause uncontrolled bioaccumulations. This constitutes a great risk for the water environment and for human health.

The antibiotics, sulfonamides, are used throughout the world, and to remove sulfanomides several methods have recently been used such as ion exchange, membrane filtration ozonation and adsorption.<sup>[3–6]</sup> Ozonation is extremely successful in removing sulfanomides but ozone can form a potent cancerogenous bromate ion. The use of other removal technologies for

sulfanomides such as membrane separation and photocatalysis are limited by high costs and complex design and operation. When all these factors are taken into consideration, adsorption has become attractive for the removal of organic chemicals from aqueous solutions because of advantages such as high efficiency, simple operation and low toxicity.<sup>[7]</sup>

Widely used adsorbents for the removal of antibiotics in the adsorption technique include active carbons (AC), carbon nanotubes, bentonite, biochars (BC), magnetic nanoparticles (MNP), active carbon composites, and magnetic biochars (MBC).<sup>[8–11]</sup> MBC is a type of biochar composite material loaded with magnetic materials, so that they not only retain the excellent properties of biochars but also have magnetic properties. BC has a high clearance capacity for organic and inorganic pollutants from an aqueous solution and can only be separated from water with traditional sedimentation, filtration, coagulation, and treatment processes.<sup>[12,13]</sup> These procedures are generally costly or ineffective, which limits application to a great extent.<sup>[14,15]</sup> MBCs can overcome the above-mentioned problems due to the magnetic separation properties and re-use is possible. All the raw materials used to produce BC can be used to prepare MBC.<sup>[16–18]</sup>

The *Punica Granatum*, commonly known as the pomegranate, is wasted as a potential biomass to a great extent as most of the inedible remains are discarded. To date, there have been few studies in literature related to biochar

obtained from pomegranate peel and its application, and there are no studies of MBC obtained from pomegranate peel and its application.<sup>[19–21]</sup>

In this study, pomegranate waste was used to prepare MBC. MBC (Fe<sub>3</sub>O-BCPP) was synthesized with the impregnation method from iron oxide nanoparticles with biochar obtained from pomegranate peel. The efficacy of the adsorbent obtained was investigated for the removal of sulfadiazine (SDZ), which is in the sulfonamide group. The synthesized MBC was characterized with a scanning electron microscope (SEM), x-ray diffraction device (XRD), vibrating sample magnetometer (VSM) and (Brunauer–Emmett–Teller) BET analysis. To determine the efficacy of Fe<sub>3</sub>O<sub>4</sub>-BCPP in eliminating SDZ, a detailed examination was made of parameters which affect adsorption efficacy such as pH, the amount of adsorbent, the duration of adsorption and the adsorption capacity. Thus, under the defined optimum conditions, the efficacy of Fe<sub>3</sub>O<sub>4</sub>-BCPP in removing SDZ from waste water, river water, and tap water was investigated.

## Materials and methods

### Materials

All the chemical used in this study were of analytical purity and were used by dissolving in deionized water (18.2 MΩ). For the synthesis of magnetic nanoparticles, FeCl<sub>3</sub>·6H<sub>2</sub>O (99%, Merck), FeSO<sub>4</sub>·7H<sub>2</sub>O (≥99.5–104.5%, Sigma Aldrich) and ammonium hydroxide (26%, Sigma Aldrich) were used. SDZ was prepared with dissolution within a stock solution of sulfadiazine sodium salt (≥98% HPLC, Sigma Aldrich) 0.01 M sodium hydroxide (≥98.0–100.5% pellets, Sigma Aldrich). In the adsorption assays, the pH settings of the solutions were made with 0.1 M hydrochloric acid (36.5–38%, Sigma Aldrich) and 0.1 M sodium hydroxide solutions. Acetonitrile and formic acid were purchased from Sigma Aldrich.

### Instrument

To determine surface morphology of Fe<sub>3</sub>O<sub>4</sub> magnetic particles, SEM images (Tescan Mira III, Czech) were applied. X-ray diffraction spectrometry (XRD) was performed by the device Pananalytical- XRD with X-ray radiation of Cu Kα anode with an angle of 10–70° (X-rays with the wavelength of 1.54056 Å). The magnetization curves of the Fe<sub>3</sub>O<sub>4</sub>-BCPP were measured using a vibrating sample magnetometer (Lake Shore 7406). Specific surface area was obtained and calculated according to the Brunauer Emmette Teller (BET) method.

UV–VIS spectrophotometer (Shimadzu 3600, Japan) was used for all absorbance measurements. Concentration of SDZ in the real sample was analyzed using high performance liquid chromatography (HPLC) with UV detector (wavelength: at 270 nm). Agilent 1100 series HPLC system equipped with a degasser (G1322A), a gradient pump (G1311A, QuadPump), a manual injector (Rheodyne 7725i) with a 20 µL loop volume, a column oven (G1316A), and an ultraviolet detector (G1314A) was used in this study. The analytical separation was performed by a stainless steel C18 analytical column (Prontosil, 250 × 4.6 mm, 5 µm, Bischoff Chromatography, Germany)

### Preparation of adsorbent

#### Biochar production from pomegrate peel

Pomegrate peel (PP) were washed with deionized water and dried in an oven for 24 h at 60°C. It was then ground and sieved to particle sizes ranging from ≥ 0.5 mm. In order to biochar KOH and pomegranate peel were mixed with a ratio of 3:1 and was carbonized in a muffle furnace at 500 C for 2 h. Pomegranate peel biochar (BCPP) was washed several times with deionized water until neutralized and it was dried in oven at 80°C for 2 h.<sup>[22]</sup>

#### Preparation of magnetic nanoparticles

To synthesize magnetic nanoparticles (Fe<sub>3</sub>O<sub>4</sub>), 6.1 g FeCl<sub>3</sub>·6H<sub>2</sub>O was dissolved in 100 mL deionized water, then a few drops of concentrated HCl (37%) were added to prevent Fe(OH)<sub>3</sub> precipitation, then 4.2 g FeSO<sub>4</sub>·7H<sub>2</sub>O was added and heated to 90°C previously reported.<sup>[23–27]</sup> Then, 20 mL of NH<sub>3</sub> (26%) was added to this solution rapidly. The mixture was stirred at 90°C for 30 minutes, then cooled to room temperature. The resulting solid black matter was collected by strong magnet, washed several times with ethanol and deionized water. The resulting Fe<sub>3</sub>O<sub>4</sub> was dried at 60°C.

#### Preparation of magnetic biochar

Separately, 0.5 gram BCPP and 0.5 gram Fe<sub>3</sub>O<sub>4</sub> were added to 50 mL ethanol in erlenmeyer and sonicated for 1 h into bath water. Then, this suspensions were combined and the mixture was sonicated for 8 min and subsequently was shaken for 12 h at 250 rpm. The obtained product (Fe<sub>3</sub>O<sub>4</sub>-BCPP) were collected at the edge of the erlenmeyer by magnet and liquid phase decanted. Fe<sub>3</sub>O<sub>4</sub>-BCPP was washed with deionized water and dried in an oven at in 80 C for 12 h.<sup>[28,29]</sup>

## Adsorption procedure

Adsorption experiments were conducted with 50 mg  $\text{Fe}_3\text{O}_4$ -BCPP adsorbent in 50 mL (10 mg/L SDZ) which were shaken at 50 rpm and 25°C for approximately 15 minutes. After adsorption, the adsorbent was separated by a powerful magnet. The factors influencing adsorption including the initial pH, amount of MBCs, initial concentration, and adsorption time were investigated. The concentration of the SDZ in supernatant was analyzed to calculate the removal efficiency and the adsorption ability. Each experiment was repeated at least three times and experiment results were given with their mean and standard deviations.

The concentration of the model solutions were measured by UV-vis spectrophotometer at 270 nm and calculated based on a calibration curve. The SDZ real samples were analyzed by HPLC with a UV detector (wavelength: at 270 nm). The mobile phase for determining SDZ s was a mixture solution containing % 0.1 formic acid and acetonitrile (30/70, v/v). The injection volume of the sample was 20  $\mu\text{L}$  and the flow rate was 1 mL/min with the isocritical mode when separation was achieved at 30°C. The total run time was 5 min. The correlation coefficient ( $R^2$ ) of the standard curve generated was  $\geq 0.9972$ .

The removal % SDZ was calculated by the following equation

$$\%R = (C_0 - C_e/C_0) \times 100$$

where  $C_0$  (mg/L) and  $C_e$  (mg/L) are the initial and equilibrium concentrations of an antibiotic stock solution.

## Results and discussion

### Characterization of $\text{Fe}_3\text{O}_4$ -PPBC

The SEM images of PP, BCPP and  $\text{Fe}_3\text{O}_4$ -BCPP were given Fig. 1. The SEM images was shown that biochar was successfully modified with  $\text{Fe}_3\text{O}_4$ . As seen in Fig. 1a, PP has a smooth surface. Figure 1b, PPBC which is the biochar obtained from PP has a porous structure and roughness surface. It is seen that the morphological structure of BCPP changes with the loading of iron oxide particles and iron oxide particles are embedded in the pores of the BCPP in Fig. 1c.

The main elements present in  $\text{Fe}_3\text{O}_4$ -BCPP before and after adsorption of SDZ ( $\text{C}_{10}\text{H}_{10}\text{N}_4\text{O}_2\text{S}$ ) are determined by EDS analysis and their spectra are shown in Figure S1. The results indicated that the carbon, nitrogen, oxygen, potassium and iron were the main elements present in  $\text{Fe}_3\text{O}_4$ -BCPP structure with percent composition as 56.82%, 0.85%, 27.27%, 0.52% and 14.55% by weight respectively. The results after adsorption of SDZ indicated that the carbon, nitrogen, oxygen, potassium iron and sulfur were contains percent composition as 48.61%, 6.38%, 22.92%, 0.41%, 21.05% 0.64% by weight respectively. In the EDS spectrum of after adsorption of SDZ the difference in the composition percentage of the element N and the presence of the element S indicate the adsorption of SDZ on  $\text{Fe}_3\text{O}_4$ -BCPP.

The magnetization curve of  $\text{Fe}_3\text{O}_4$ -BCPP was given in Fig. 2. The saturation magnetization of  $\text{Fe}_3\text{O}_4$ -BCPP was 12.5 emu/g (Fig. 2b). As seen in the magnetization curve,  $\text{Fe}_3\text{O}_4$ -BCPP has superparamagnetic properties and  $\text{Fe}_3\text{O}_4$ -BCPP from aqueous dispersions could be easily separated by an external magnet.

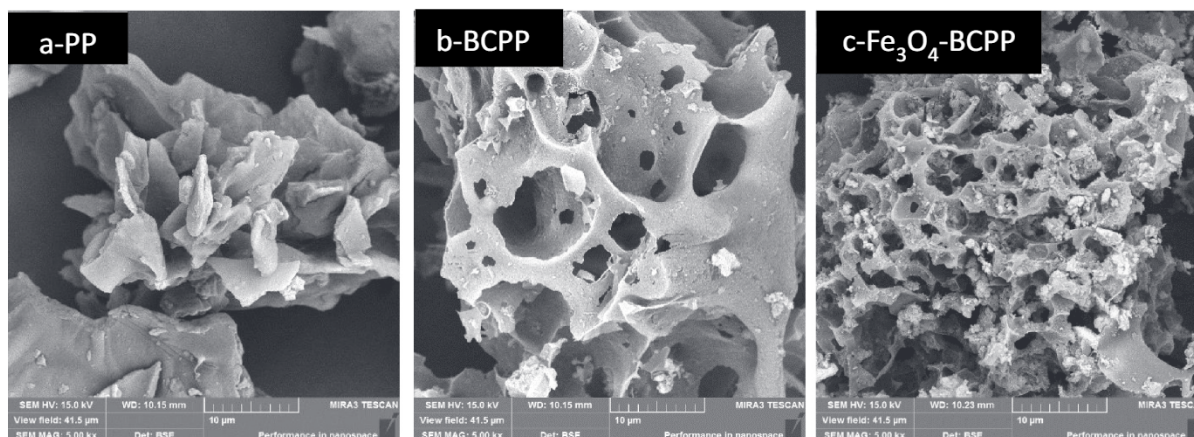
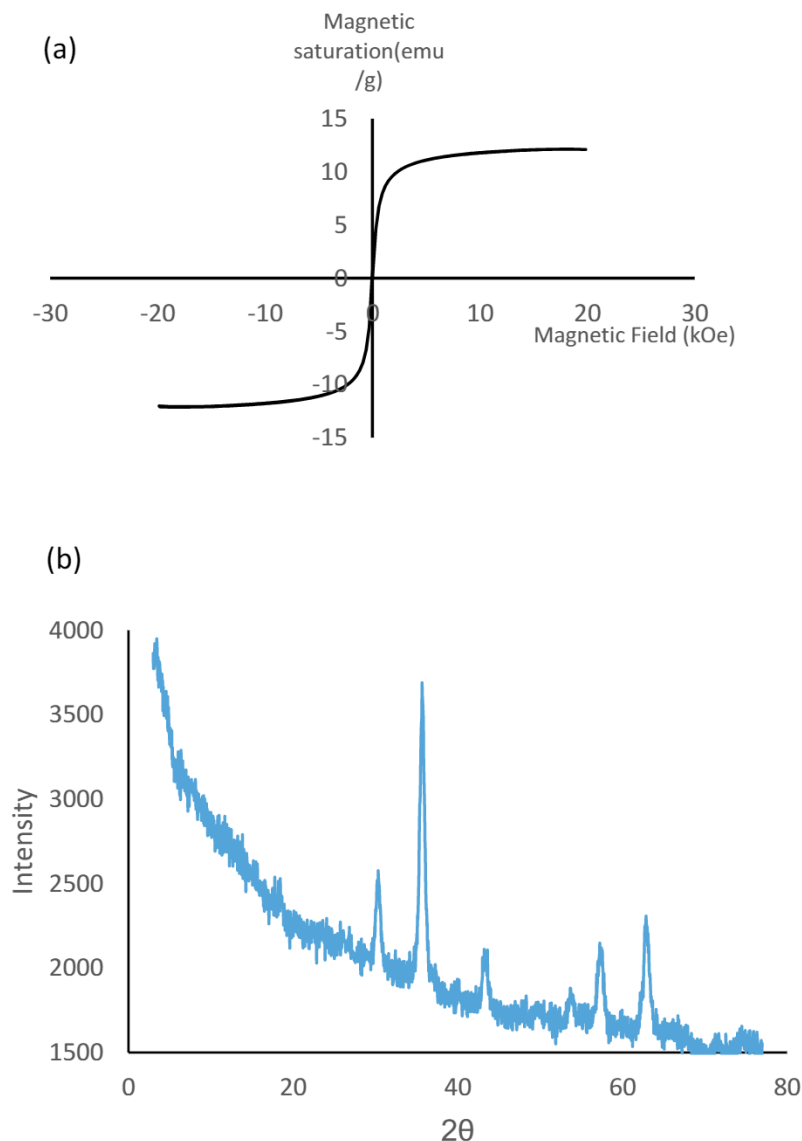


Figure 1. SEM images of PP(a), BCPP (b) and  $\text{Fe}_3\text{O}_4$ -BCPP (c).



**Figure 2.** A.The magnetization curve of  $\text{Fe}_3\text{O}_4$ -BCPP b. XRD pattern of  $\text{Fe}_3\text{O}_4$ -BCPP.

Figure 2b shows X-ray powder diffraction pattern of  $\text{Fe}_3\text{O}_4$ -BCPP. As seen in the Fig. 2b the peaks were obtained 30.3 (220), 35.7 (311), 43.3 (400), 54.1 (422), 57.3 (511) and 62.9 (440).<sup>[25,30]</sup>

These series of characteristic peaks is show that the major composition of MNP belongs to  $\text{Fe}_3\text{O}_4$  (magnetite). The average nanoparticle diameter (D) for  $\text{Fe}_3\text{O}_4$ -BCPP was calculated according to following Debye–Scherrer equation.

$$D_{HKL} = \frac{k\lambda}{B(2\theta) \cdot \cos\theta}$$

Here, D is the mean nanoparticle diameter  $\lambda$ ; X-rays wavelength, B ( $2\theta$ ); half maximum width of the corresponding peak,  $\theta$ : corresponding is the angle of the peak.

The average nanoparticle diameter of  $\text{Fe}_3\text{O}_4$ -BCPP was calculated as 11.5 nm using the peak with a  $2\theta$  value of  $35.7^\circ$  which is the most intense peak.

The BET surface area, pore volume and pore size were measured by BJH method. The BET specific surface of BCPP and  $\text{Fe}_3\text{O}_4$ -BCPP were  $526.6 \text{ m}^2/\text{g}$  and  $247.0$  respectively (Table 1). BCPP has a larger specific surface area than  $\text{Fe}_3\text{O}_4$ -BCPP. However, disadvantage of BCPP for SDZ removal is the difficulty of separating it from solution, which is a common problem for powdered adsorbent. This problem has been overcome with the  $\text{Fe}_3\text{O}_4$ -BCPP (magnetic composite) which can be easily separated from the solution by a magnetic field.

In order to determine the point of zero charge (pzc) of  $\text{Fe}_3\text{O}_4$ -BCPP, 50 mg adsorbent ( $\text{Fe}_3\text{O}_4$ -BCPP) was added to 50 mL model solutions which pH was adjusted

with nitric acid and NaOH in the range of 2–10 and shaken for 24 hours. At the end of 24 hours, the pH of the solutions was measured. The changes of the pH ( $\Delta\text{pH}$ ) were plotted against the initial pH. The graph is given Figure S2. The point where the plot bisects the x-axis was corresponding to the pzc of  $\text{Fe}_3\text{O}_4\text{-BCPP}$ . The  $\text{pH}_{\text{pzc}}$  of the  $\text{Fe}_3\text{O}_4\text{-BCPP}$  is found to be  $\text{pH} = 5.7$ . This indicates that in pH values below the  $\text{pH} = 5.7$  the  $\text{Fe}_3\text{O}_4\text{-BCPP}$  surface is positively charged and at pH values higher than the  $\text{pH}_{\text{pzc}}$ , the  $\text{Fe}_3\text{O}_4\text{-BCPP}$  surface is negatively charged.

### Factors influencing adsorption

#### The effect of the solution pH on adsorption of SDZ

In the adsorption process, the initial pH of the solution is one of the parameters with a significant effect on the efficacy of adsorption, because the pH of the solution affects the surface load of the adsorbents and the degree of ionization of the analytes. In this study, the effect of pH values between 2 and 6 was examined. To determine the effect of pH in the adsorption process, model solutions were prepared containing 100 mg  $\text{Fe}_3\text{O}_4\text{-BCPP}$  in 50 ml varying in pH range of 2–6 and at an initial concentration of 10 mg/L. The adsorption process was applied at room temperature, at a mixing rate of 50 rpm, for 15 mins. The assay results are shown in Fig. 3. Sulfadiazine may exist as cationic, neutral, and anionic species, depend on the pH of the aqueous phase. Sulfadiazine exists mainly in the cationic form for  $\text{pH} < 1.57$  and mainly anionic form for  $\text{pH} > 6.50$ . The neutral form of sulfadiazine is prevalent when pH values are between 1.57 and 6.50.<sup>[31,32]</sup> As the pH of the solution increases, the ratio of neutral to the cationic form of sulfadiazine increases and in the pH range of 2–4 the interaction of analyte and adsorbent reaches its

maximum, resulting in higher removal efficiency. When  $\text{pH} > 5.0$  the anionic form of sulfadiazine increases and the removal efficiency decreases as a consequence of the repulsion with negatively charged  $\text{Fe}_3\text{O}_4\text{-BCPP}$ . Therefore, in the subsequent experiments, a pH value of 3 was selected as optimum.

#### The effect of the amount of adsorbent

One of the parameters affecting the efficacy of adsorption is the amount of sorbent used. The efficacy of sorbent used at amounts of 0.5 g/L, 1.0 g/L, and 2 g/L was examined, and the percentage removal of 10 mg/L SDZ was seen to be  $83 \pm 2.2\%$  for 0.5 g/L,  $101 \pm 0.3\%$  for 1 g/L and  $97 \pm 0.7\%$  for 2 g/L. Therefore, the subsequent experiments were conducted using 50 mg sorbent in 50 mL solution.

#### The effect of contact time and initial concentration of SDZ on adsorption

To examine the effect of initial concentration and contact time of adsorption of SDZ with  $\text{Fe}_3\text{O}_4\text{-BCPP}$ , time-dependent experiments were conducted with 50 mg adsorbent at 50rpm mixing speed using 50 mL model solutions of pH 3 containing SDZ at 50, 100, and 200 mg/L. The changes occurring in adsorption at the defined time intervals are shown in Fig. 4. The 50 mg/L SDZ clearance rate was 90% in 20 mins, and 95% after 60 mins. The SDZ adsorption with  $\text{Fe}_3\text{O}_4\text{-BCPP}$  was seen to stabilize after 60 mins.

#### Desorption and Re-use

The re-use of adsorbents is an important indicator in the determination of the potential for commercial applications. In the SDZ desorption studies, reactive 10%  $\text{NH}_3$ , methanol, 10%  $\text{NH}_3\text{-Methanol}$  and 15%  $\text{NH}_3\text{-Methanol}$  solutions were used. 50 mg adsorbent

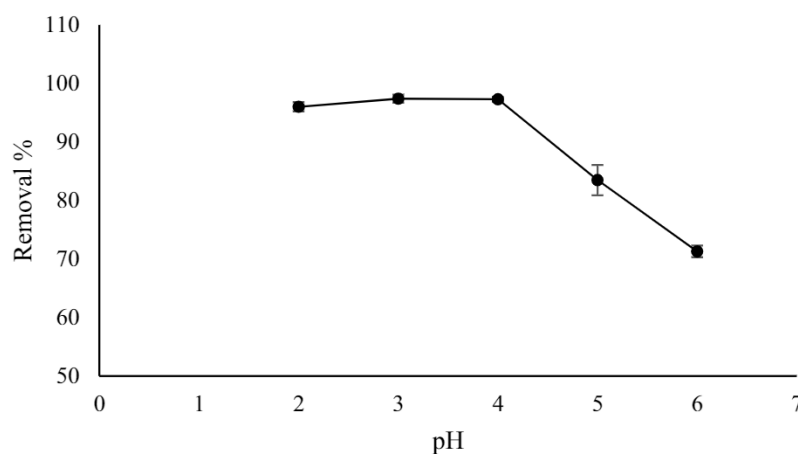
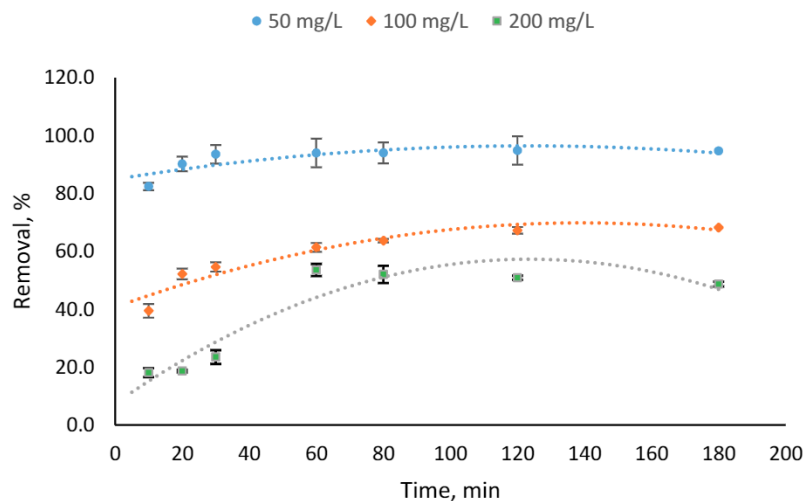


Figure 3. The effect of the solution pH on adsorption of SDZ ( $C_0 = 10$  mg/L, contact time = 15 min, amount of adsorbent = 2 g/L).



**Figure 4.** Effect of contact time and initial concentration of SDZ on the adsorption (pH: 3, amount of adsorbent = 1 g/L).

was added to the 50 mL model solution of pH 3 containing 10 mg/L SDZ and this was mixed for 15 min at 50 rpm. The  $\text{Fe}_3\text{O}_4$ -BCPP which had adsorbed SDZ was separated from the solution using a magnet and the liquid phase was discarded with decantation. Then 50 mL desorption solution was added to the magnetic biochar, and this was mixed for 2 hours. The SDZ concentration in the desorption solution was measured with UV-VIS spectrophotometry. With 101% of SDZ recovered from  $\text{Fe}_3\text{O}_4$ -BCPP with 15%  $\text{NH}_3$ -Methanol, this was seen to be a good desorption solution. The recovery percentages of the solutions used for desorption of SDZ from  $\text{Fe}_3\text{O}_4$ -BCPP are shown in Table 2.

The re-usability of  $\text{Fe}_3\text{O}_4$ -BCPP was investigated with 9 consecutive adsorption/desorption cycles (Fig. 5). After 4 adsorption/desorption cycles, the SDZ adsorption efficiency obtained was  $94 \pm 2\%$  and desorption  $84 \pm 4\%$ . The adsorption-desorption experiments were repeated with a desorption time of 3 hours and at the end

of 4 cycles SDZ was observed to be  $100 \pm 4\%$  desorbed. In the following cycles, the adsorption time was fixed at 15 mins and the desorption time of 3 hours was used. After the 7th, 8th, and 9th adsorption-desorption cycles, the mean SDZ desorption was found to be  $85 \pm 3\%$  and desorption  $88 \pm 2\%$ . The re-usability of the adsorbent was seen to remain stable after the 7th cycle.

### Adsorption kinetics

To determine what type of role is played by the mechanism characterizing the adsorption process, the so-called first degree kinetic model and so-called second degree kinetic model were used.<sup>[33–35]</sup>

For the so-called first degree kinetic model, generally the following equation is used:  $\ln(q_e - q_t) = \ln q_e - k_1 t$

For the so-called second degree kinetic model, generally the following equation is used:  $t/q_e = 1/k_2 q_e^2 - t/q_e$

**Table 1.** Surface area and pore characteristics of BCPP and  $\text{Fe}_3\text{O}_4$ -BCPP.

Surface Properties			
	BET surface area $\text{m}^2/\text{g}$	Pore volume $\text{cm}^3/\text{g}$	Pore Radius nm
BCPP	526.6	0.06	1.89
$\text{Fe}_3\text{O}_4$ -PPBC	247.0	0.13	4.71

**Table 2.** Desorption solution (n = 3).

Desorption Solution	% Recovery
Methanol	$56 \pm 1$
%10 $\text{NH}_3$ in water	$77 \pm 2$
%10 $\text{NH}_3$ in methanol	$85 \pm 2$
% 15 $\text{NH}_3$ in methanol	$101 \pm 4$

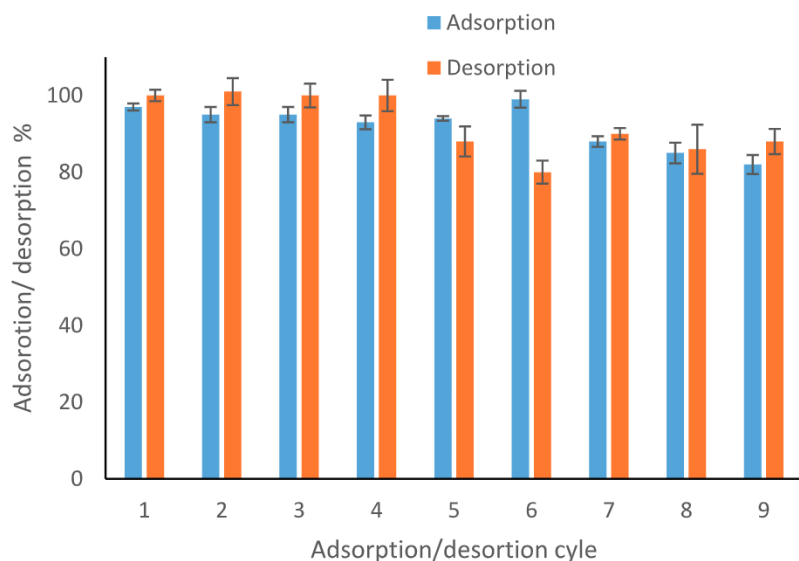


**Figure 5.** Adsorption and desorption cycle (pH: 3, amount of adsorbent = 1 g/L, adsorption time: 15 min, desorption time: 3 h).

In these,  $q_e$  and  $q_t$  represent the amount of material adsorbed (mg/g) in balance and in  $t$  time,  $k_1$  indicates first degree adsorption fixed rate ( $\text{min}^{-1}$ ), and  $k_2$  indicates second degree adsorption fixed rate (g/mg. min).

For the so-called first degree kinetic model, the  $k_1$  and  $q_e$  values were calculated with the cutoff point of the  $y$  axis and the linear relationship curve obtained by plotting the  $1/n$  value ( $q_e - q_t$ ) against  $t$ .

For the so-called second degree kinetic model, the  $q_e$  and  $k_2$  values were calculated with the cutoff point of the  $y$  axis and the linear relationship curve obtained by plotting the  $t/q_t$  value against  $t$ .

The adsorption kinetic data defined in the so-called first and second degree kinetic models are shown in Table 3. The choice of the suitable kinetic model was adjudged by comparing the error analysis values and correlation coefficients ( $R^2$ ). As seen in the Table 3, the  $R^2$  values for  $\text{Fe}_3\text{O}_4$ -BCPP for the first model were found to be 0.709 and 0.684, respectively. The correlation coefficient for the data of this model was low, so it was

concluded that this was not an appropriate model. The  $R^2$  values for  $\text{Fe}_3\text{O}_4$ -BCPP for the second model were found to be 0.9999 and 0.9374, respectively. The higher correlation coefficients and lower error values for  $\text{Fe}_3\text{O}_4$ -BCPP adsorption of SDZ showed that the second degree kinetic model was suitable. Error functions for kinetic models and their mathematical formula were given in Table 4 and Table S1 respectively

This kinetic model is based on the assumption that the speed limiting stage could be chemical adsorption involving balancing forces through the exchange or sharing of electrons between the adsorbent and adsorbate.

### Adsorption capacity

Adsorption isotherm studies are of fundamental importance in the determination of the SDZ adsorption capacity of  $\text{Fe}_3\text{O}_4$ -BCPP. Balance data have been investigated using Langmuir, Freundlich and Temkin isotherm models. While Langmuir accepts that adsorption isotherm is single layer adsorption on a homogenous surface, Freundlich isotherm refers to the Temkin adsorption model on heterogeneous surfaces, as chemical adsorption

**Table 3.** The kinetic parameters for  $\text{Fe}_3\text{O}_4$ -BCPP adsorption of SDZ ( $n = 3$ ).

Error functions	Kinetic models	
	Pseudo-first order model	Pseudo-second order model
Sum of the squares of errors (SSE)	6.454	0.971
Sum of absolute errors (EABS)	4.260	1.780
The mean square error (MSE)	1.076	0.162
Root means square error (RMSE)	1.136	0.441
Cie square ( $X^2$ )	$2.86 \times 10^{-3}$	$4.54 \times 10^{-4}$

**Table 4.** Error functions for kinetic models.

SDZ concentration (mg/L)	Pseudo-first order rate parameter			Pseudo-second order rate parameter		
	$q_e$ (mg/g)	$k_1$ ( $\text{min}^{-1}$ )	$R^2$	$q_e$ (mg/g)	$k_2$ ( $\text{min}^{-1}$ )	$R^2$
50	4.05	0.035	0.7086	47.62	0.019	0.9999
200	11.06	0.017	0.6840	64.94	$1.44 \times 10^{-4}$	0.9374



based on powerful electrostatic interaction between positive and negative loads.<sup>[34,36,37]</sup> The Langmuir model is stated with the linear equation below:

$$\frac{C_e}{q_e} = \frac{1}{q_{\max}b} + \frac{C_e}{q_{\max}}$$

In this,  $q_e$ (mg/g) indicates the amount of analyte adsorbed per unit of sorbent mass in the balanced solution,  $C_e$ (mg/L) is the concentration of analyte in the balanced solution,  $q_{\max}$ (mg/g) is the maximum amount of analyte adsorbed per unit of sorbent mass, and  $b$  (L/mg) is a constant associated with the affinity of the binding regions.

$q_{\max}$  and  $b$  Langmuir constants are calculated from the curve of the linear graph drawn between  $C_e$  and  $C_e/q_e$  and the shift values.

The Freundlich linear equation is expressed as:

$$\ln q_e = \ln K_f + \frac{1}{n} \ln C_e$$

In this, the  $K_f$  (L/g) and  $n$  Freundlich constants are adsorbent capacity and heterogeneity factor, respectively. The  $\kappa F$  and  $\eta$  values are calculated from the curve and cutoff point of the linear graph drawn according to  $\ln q_e$  and  $\ln C_e$ .

The following equation is used for the Temkin isotherm model:

$$q_e = \frac{RT}{b} \ln A + \frac{RT}{b} \ln C_e$$

In this, the  $B_T = RT/b$  constant is related to the adsorption temperature,  $R$  is the gas constant (8.314 J/mol K),  $T$  (K) is the absolute heat in Kelvin units, and  $b$  (J/mol) is the Temkin isotherm constant and adsorption energy variable.

$A$  is the balance binding constant corresponding to maximum binding energy. Both  $B_T$  and  $A$ , are calculated from the curve and cutoff point of the linear graph based on  $\ln(C_e)$  and corresponding to  $q_e$ .

The isotherm constants and correlation coefficients ( $R^2$ ) are shown in Table 5 and graphs of adsorption isotherm Figure S3. The experiment data related to the correlation coefficients showed that the  $Fe_3O_4$ -BCPP adsorption of SDZ was consistent with Langmuir isotherm ( $R^2 = 0.9998$ ), demonstrating that the adsorption was homogenous and occurred in a single layer.

**Table 5.** The parameters of the langmuir, freundlich and temkin models for SDZ adsorption.

Langmuir			Freundlich			Temkin		
$q_{\max}$	$b$	$R^2$	$K_f$	$n$	$R^2$	$B_t$	$A_t$	$R^2$
(mg/g)	(L/mg)		(mg/g)					
			(L/mg) <sup>1/n</sup>					
95.2	1.3	0.9998	1.1 <sup>-6</sup>	0.3	0.9202	9.4	49.2	0.9921

Separation constant ( $R_L$ ) is one of the most important parameters of the Langmuir isotherm.  $R_L$  is calculated as given by the following equation,

$$R_L = \frac{1}{1 + bC_0}$$

where  $C_0$  is initial concentration of the adsorbate and  $b$  is a Langmuir isotherm constant. In this regard, separation constants were calculated as 0.004–0.038 for different concentrations SDZ. The  $R_L$  value between 0 and 1 indicates that the adsorption process is favorable.<sup>[38]</sup>

Comparisons of  $Fe_3O_4$ -BCPP with other adsorbents are listed in Table 6. The SDZ adsorption capacity of  $Fe_3O_4$ -BCPP was seen to be at a comparable level with other adsorbents. The adsorption duration of  $Fe_3O_4$ -BCPP was seen to be comparable and better when compared to other adsorbents.

### Effect of interferences

In order to understand the applicability of the proposed MSPE in the real field, the effects of organic and inorganic pollutants on SDZ removal were investigated. Interfering components and their concentrations have been selected taking into account the the current previous wastewater studies in literature.<sup>[45,46]</sup> These components were added to solutions of 50 mL containing 10 mg/L SDZ as their chloride, nitrate, sulfate and salts within the range of 50–3000 mg/L. The proposed MSPE method was applied. The obtained results are shown in Table 7. The results demonstrate that the developed method is suitable for the removal of SDZ from water samples.

**Table 6.** Comparison of  $Fe_3O_4$ -BCPP with previously studied adsorbents.

Adsorbents	capacity (mg/g)	Adsorbent g/L	pH	Adsorption Time (h)	Reference
CSB-6-2.5	86.89	1	4	12	[32]
Coffee grounds derived biochar	0.22	3.33	6.8	24	[39]
amino-functionalized porous carbon materials	124.6	0.1	-	12	[40]
Multi-walled carbon nanotubes	132.33	1	3	2	[41]
MMWCNTs-MIP	48.4	0.2	4	1	[42]
Glucose-based mesoporous carbon	246.73	0.25	4	2	[43]
silica ZSM-5	6.21	0.2	4.4	48	[44]
$Fe_3O_4$ -BCPP	95.2	1	3	1	This Study

**Table 7.** Effect of interfering ions on the removal of SDZ (n = 3).

Substance/ion	Salt	Concentration (mg/L)	Removal %
Ca <sup>2+</sup>	Ca(NO <sub>3</sub> ) <sub>2</sub> · 4H <sub>2</sub> O	1000	96.4 ± 0.1
Mg <sup>2+</sup>	Mg(NO <sub>3</sub> ) <sub>2</sub> · 6H <sub>2</sub> O	1000	97.8 ± 0.3
K <sup>+</sup>	KCl	1000	98.7 ± 0.7
Na <sup>+</sup>	NaCl	1000	99.4 ± 0.2
Cl <sup>-</sup>	NaCl	1500	99.4 ± 0.2
NO <sub>3</sub> <sup>-</sup>	Ca(NO <sub>3</sub> ) <sub>2</sub> · 4H <sub>2</sub> O	3000	97.8 ± 0.3
SO <sub>4</sub> <sup>2-</sup>	Na <sub>2</sub> SO <sub>4</sub>	500	98.2 ± 0.6
HCO <sub>3</sub> <sup>-</sup>	NaHCO <sub>3</sub>	500	99.7 ± 0.3
CH <sub>3</sub> COO <sup>-</sup>	NH <sub>4</sub> CH <sub>3</sub> COO	500	99.8 ± 0.3
Glucose	-	1000	96.6 ± 0.3
Urea	-	100	98.2 ± 0.1
Peptone	-	50	93.4 ± 0.4
Starch	-	150	97.6 ± 0.8

**Table 8.** The efficiency of Fe<sub>3</sub>O<sub>4</sub>-BCPP in removing SDZ from real water samples (pH:3, amount of sorbent:1 g/L, Adsorption time: mixing at 50 rpm for 1 hour).

	SDZ (mg/L)	
	10	20
Tap Water	95.6 ± 0.3	85.2 ± 0.2
River	96.1 ± 0.2	86.2 ± 2.8
Sea Water	96.5 ± 0.9	87.5 ± 0.5
Waste Water	47.6 ± 2.5	42 ± 0.9

### Removal of SDZ from real water samples

The determination of the adsorption efficacy of sorbents in real water samples is very important economically and to be able to implement sustainable water treatment applications.<sup>[47]</sup> Therefore, the efficacy of the recommended procedure in real samples was investigated by applying it to samples of tap water, river water, waste water, and sea water. The recommended adsorption method was applied to 100 mL water samples and water samples with additives under optimum conditions. The efficacy of the removal of SDZ from different water samples is shown in Table 8.

As seen in the table, the removal percentages for the tap water and river water samples with 10 mg/L and 20 mg/L added SDZ were 85.2 ± 0.2% and 96.1 ± 0.2%, respectively. That similar removal percentages were obtained for the SDZ spiked sea water samples shows that the method was not affected by the high salt content. However, the results showed lower removal efficacy in the waste water samples. As waste water has complex chemical components and microbial populations, this can be said to have significantly affected the efficacy of SDZ removal. The chromatograms of the real sample applications are given in Figure S4.

### Conclusion

The results of this study demonstrated that Fe<sub>3</sub>O<sub>4</sub>-BCPP as the magnetic adsorbent can be used effectively at low cost for the clearance of SDZ from water samples and

has good potential for application. The maximum SDZ adsorption capacity of Fe<sub>3</sub>O<sub>4</sub>-BCPP was found to be 95.2 mg/g. Fe<sub>3</sub>O<sub>4</sub>-BCPP has the important advantages of high adsorption capacity, good re-usability, and a short adsorption time. Moreover, Fe<sub>3</sub>O<sub>4</sub>-BCPP obtained from pomegranate peel can be used as a promising and effective adsorbent for the clearance of various other pollutants in the improvement of waste water treatment facilities and the environment.

### Acknowledgements

This study is supported by the Scientific Research Project Fund of Sivas Cumhuriyet University under the Project number ECZ-2021-081. HPLC analyzes were conducted at Sivas Cumhuriyet University Faculty of Medicine Research Center (CÜTFAM). The authors thank the CÜTFAM staff for their open collaboration.

### Disclosure statement

No potential conflict of interest was reported by the author(s).

### References

- [1] Ahmed, M. B.; Zhou, J. L.; Ngo, H. H.; Guo, W. Adsorptive Removal of Antibiotics from Water and Wastewater: Progress and Challenges. *Sci. Total Environ.* **2015**, *532*, 112–126. DOI: [10.1016/j.scitotenv.2015.05.130](https://doi.org/10.1016/j.scitotenv.2015.05.130).
- [2] Zhong, J.; Feng, Y.; Li, J. L.; Yang, B.; Ying, G. G. Removal of Sulfadiazine Using 3D Interconnected petal-like Magnetic Reduced Graphene Oxide (Mrgo) Nanocomposites. *Water (Switzerland)*. **2020**, *12*. DOI: [10.3390/w12071933](https://doi.org/10.3390/w12071933).
- [3] Dao, T. H.; Tran, T. T.; Nguyen, V. R.; Pham, T. N. M.; Vu, C. M.; Pham, T. D. Removal of Antibiotic from Aqueous Solution Using Synthesized TiO<sub>2</sub>nanoparticles: Characteristics and Mechanisms. *Environ. Earth Sci.* **2018**, *77*(10), 1–14. DOI: [10.1007/s12665-018-7550-z](https://doi.org/10.1007/s12665-018-7550-z).
- [4] Guo, R.; Chen, J. Application of alga-activated Sludge Combined System (AASCS) as a Novel Treatment to Remove Cephalosporins. *Chem. Eng. J.* **2015**, *260*, 550–556. DOI: [10.1016/j.cej.2014.09.053](https://doi.org/10.1016/j.cej.2014.09.053).
- [5] Saravanan, R.; Sacari, E.; Gracia, F.; Khan, M. M.; Mosquera, E.; Gupta, V. K. Conducting PANI Stimulated ZnO System for Visible Light Photocatalytic Degradation of Coloured Dyes. *J. Mol. Liq.* **2016**, *221*, 1029–1033. DOI: [10.1016/j.molliq.2016.06.074](https://doi.org/10.1016/j.molliq.2016.06.074).
- [6] Sánchez-Polo, M.; Rivera-Utrilla, J.; Prados-Joya, G.; Ferro-García, M. A.; Bautista-Toledo, I. Removal of Pharmaceutical Compounds, Nitroimidazoles, from Waters by Using the ozone/carbon System. *Water Res.* **2008**, *42*(15), 4163–4171. DOI: [10.1016/j.watres.2008.05.034](https://doi.org/10.1016/j.watres.2008.05.034).

- [7] Vallinayagam, S.; Rajendran, K.; Lakkaboyana, S. K.; Soontarapa, K.; R, R.; Sharma, R.; K, V.; Kumar, V.; Venkateswarlu, K.; Koduru, J. R. Recent Developments in Magnetic Nanoparticles and nano-composites for Wastewater Treatment. *J. Environ. Chem. Eng.* **2021**, *9* (6), 106553. DOI: [10.1016/j.jece.2021.106553](https://doi.org/10.1016/j.jece.2021.106553).
- [8] Pouretedal, H. R.; Sadegh, N. Effective Removal of Amoxicillin, Cephalexin, Tetracycline and Penicillin G from Aqueous Solutions Using Activated Carbon Nanoparticles Prepared from Vine Wood. *J. Water Process. Eng.* **2014**, *1*, 64–73. DOI: [10.1016/j.jwpe.2014.03.006](https://doi.org/10.1016/j.jwpe.2014.03.006).
- [9] Putra, E. K.; Pranowo, R.; Sunarso, J.; Indraswati, N.; Ismadji, S. Performance of Activated Carbon and Bentonite for Adsorption of Amoxicillin from Wastewater: Mechanisms, Isotherms and Kinetics. *Water Res.* **2009**, *43*(9), 2419–2430. DOI: [10.1016/j.watres.2009.02.039](https://doi.org/10.1016/j.watres.2009.02.039).
- [10] Fernández, A. M. L.; Rendueles, M.; Díaz, M. Sulfamethazine Retention from Water Solutions by Ion Exchange with a Strong Anionic Resin in Fixed Bed. *Sep. Sci. Technol.* **2014**, *49*(9), 1366–1378. DOI: [10.1080/01496395.2013.879666](https://doi.org/10.1080/01496395.2013.879666).
- [11] Grover, D. P.; Zhou, J. L.; Frickers, P. E.; Readman, J. W. Improved Removal of Estrogenic and Pharmaceutical Compounds in Sewage Effluent by Full Scale Granular Activated Carbon: Impact on Receiving River Water. *J. Hazard. Mater.* **2011**, *185*(2–3), 1005–1011. DOI: [10.1016/j.jhazmat.2010.10.005](https://doi.org/10.1016/j.jhazmat.2010.10.005).
- [12] Lingamdinne, L. P.; Choi, J. S.; Angaru, G. K. R.; Karri, R. R.; Yang, J. K.; Chang, Y. Y.; Koduru, J. R. Magnetic-watermelon Rinds Biochar for uranium-contaminated Water Treatment Using an Electromagnetic semi-batch Column with Removal Mechanistic Investigations. *Chemosphere.* **2022**, *286*, 131776. DOI: [10.1016/j.chemosphere.2021.131776](https://doi.org/10.1016/j.chemosphere.2021.131776).
- [13] Ahmed, W.; Mehmood, S.; Núñez-delgado, A.; Qaswar, M.; Ali, S.; Ying, H.; Liu, Z.; Mahmood, M.; Chen, D. Fabrication, Characterization and U (VI) Sorption Properties of a Novel Biochar Derived from *Tribulus Terrestris* via Two Different Approaches. *Science of the Total Environment.* **2021**, *780*. DOI: [10.1016/j.scitotenv.2021.146617](https://doi.org/10.1016/j.scitotenv.2021.146617).
- [14] Chen, B.; Chen, Z.; Lv, S. A Novel Magnetic Biochar Efficiently Sorbs Organic Pollutants and Phosphate. *Bioresour. Technol.* **2011**, *102*(2), 716–723. DOI: [10.1016/j.biortech.2010.08.067](https://doi.org/10.1016/j.biortech.2010.08.067).
- [15] Yi, Y.; Huang, Z.; Lu, B.; Xian, J.; Tsang, E. P.; Cheng, W.; Fang, J.; Fang, Z. Magnetic Biochar for Environmental Remediation: A Review. *Bioresour. Technol.* **2019**, *298*. DOI: [10.1016/j.biortech.2019.122468](https://doi.org/10.1016/j.biortech.2019.122468).
- [16] Gan, Q.; Hou, H.; Liang, S.; Qiu, J.; Tao, S.; Yang, L.; Yu, W.; Xiao, K.; Liu, B.; Hu, J., et al. Sludge-derived Biochar with Multivalent Iron as an Efficient Fenton Catalyst for Degradation of 4-Chlorophenol. *Sci. Total Environ.* **2020**, *725*, 138299. DOI: [10.1016/j.scitotenv.2020.138299](https://doi.org/10.1016/j.scitotenv.2020.138299).
- [17] Zhou, H.; Zhu, X.; Chen, B. Magnetic Biochar Supported  $\alpha$ -MnO<sub>2</sub> Nanorod for Adsorption Enhanced Degradation of 4-chlorophenol via Activation of Peroxydisulfate. *Sci. Total Environ.* **2020**, *724*, 138278. DOI: [10.1016/j.scitotenv.2020.138278](https://doi.org/10.1016/j.scitotenv.2020.138278).
- [18] Sewu, D. D.; Tran, H. N.; Ohemeng-Boahen, G.; Woo, S. H. Facile Magnetic Biochar Production Route with New Goethite Nanoparticle Precursor. *Sci. Total Environ.* **2020**, *717*, 137091. DOI: [10.1016/j.scitotenv.2020.137091](https://doi.org/10.1016/j.scitotenv.2020.137091).
- [19] Cao, Q.; Huang, Z.; Liu, S.; Wu, Y. Potential of Punica Granatum Biochar to Adsorb Cu(II) in Soil. *Sci. Rep.* **2019**, *9*(1), 11116. DOI: [10.1038/s41598-019-46983-2](https://doi.org/10.1038/s41598-019-46983-2).
- [20] Venkateswarlu, S.; Kumar, B. N.; Prathima, B.; SubbaRao, Y.; Jyothi, N. V. V. A Novel Green Synthesis of Fe<sub>3</sub>O<sub>4</sub> Magnetic Nanorods Using Punica Granatum Rind Extract and Its Application for Removal of Pb(II) from Aqueous Environment. *Arab. J. Chem.* **2019**, *12*(4), 588–596. DOI: [10.1016/j.arabjc.2014.09.006](https://doi.org/10.1016/j.arabjc.2014.09.006).
- [21] Vidovix, T. B.; Quesada, H. B.; Januário, E. F. D.; Bergamasco, R.; Vieira, A. M. S. Green Synthesis of Copper Oxide Nanoparticles Using Punica Granatum Leaf Extract Applied to the Removal of Methylene Blue. *Mater. Lett.* **2019**, *257*, 126685. DOI: [10.1016/j.matlet.2019.126685](https://doi.org/10.1016/j.matlet.2019.126685).
- [22] Wu, R. Y.; Wang, Y.; Xue, X. Y.; Hu, T. P.; Gao, J. F.; An, F. Q. Selective Adsorption and Removal Ability of Pine needle-based Activated Carbon Towards Al(III) from La(III). *J. Dispers. Sci. Technol.* **2019**, *40*(2), 186–191. DOI: [10.1080/01932691.2018.1464933](https://doi.org/10.1080/01932691.2018.1464933).
- [23] Yang, J.; Zeng, Q.; Peng, L.; Lei, M.; Song, H.; Tie, B.; Gu, J. La-EDTA Coated Fe<sub>3</sub>O<sub>4</sub> Nanomaterial: Preparation and Application in Removal of Phosphate from Water. *J. Environ. Sci.* **2013**, *25*(2), 413–418. DOI: [10.1016/S1001-0742\(12\)60014-X](https://doi.org/10.1016/S1001-0742(12)60014-X).
- [24] He, C.; Qu, J.; Yu, Z.; Chen, D.; Su, T.; He, L.; Zhao, Z.; Zhou, C.; Hong, P.; Li, Y., et al. Preparation of micro-nano Material Composed of Oyster shell/fe<sub>3</sub>o<sub>4</sub> nanoparticles/humic Acid and Its Application in Selective Removal of hg(II). *Nanomaterials.* **2019**, *9*(7), 953. DOI: [10.3390/nano9070953](https://doi.org/10.3390/nano9070953).
- [25] El-Sheikh, A. H.; Nofal, F. S.; Shtaiwi, M. H. Adsorption and Magnetic solid-phase Extraction of Cadmium and Lead Using Magnetite Modified with Schiff Bases. *J. Environ. Chem. Eng.* **2019**, *7*(4), 103229. DOI: [10.1016/j.jece.2019.103229](https://doi.org/10.1016/j.jece.2019.103229).
- [26] You, Y.; Zheng, S.; Zang, H.; Liu, F.; Liu, F.; Liu, J. ScienceDirect Stimulatory Effect of Magnetite on the Syntrophic Metabolism of Geobacter co-cultures: Influences of Surface Coating. *Geochim. Cosmochim. Acta.* **2019**, *256*, 82–96. DOI: [10.1016/j.gca.2018.02.009](https://doi.org/10.1016/j.gca.2018.02.009).
- [27] Akay, S.; Baran, T.; Kayan, B.; Kalderis, D. Assessment of a Pd – Fe<sub>3</sub>O<sub>4</sub> -biochar Nanocomposite as a Heterogeneous Catalyst for the solvent-free Suzuki-Miyaura Reaction. *Mater. Chem. Phys.* **2021**, *259*, 124176. DOI: [10.1016/j.matchemphys.2020.124176](https://doi.org/10.1016/j.matchemphys.2020.124176).
- [28] Bagheri, A. R.; Ghaedi, M.; Asfaram, A.; Bazrafshan, A. A.; Jannesar, R. Comparative Study on Ultrasonic Assisted Adsorption of Dyes from Single System onto Fe<sub>3</sub>O<sub>4</sub> Magnetite Nanoparticles Loaded on Activated Carbon: Experimental Design Methodology. *Ultrason. Sonochem.* **2017**, *34*, 294–304. DOI: [10.1016/j.ultsonch.2016.05.047](https://doi.org/10.1016/j.ultsonch.2016.05.047).

- [29] Jafari, K.; Heidari, M.; Rahmadian, O. Wastewater Treatment for Amoxicillin Removal Using Magnetic Adsorbent Synthesized by Ultrasound Process. *Ultrasonics Sonochemistry*. 2018, 45, 248–256. DOI: [10.1016/j.ultsonch.2018.03.018](https://doi.org/10.1016/j.ultsonch.2018.03.018).
- [30] El Ghandoor, H.; Zidan, H. M.; Khalil, M. M. H.; Ismail, M. I. M. Synthesis and Some Physical Properties of Magnetite (Fe<sub>3</sub>O<sub>4</sub>) Nanoparticles. *Int. J. Electrochem. Sci.* 2012, 7, 5734–5745.
- [31] Xu, J.; He, Y.; Zhang, Y.; Guo, C.; Li, L.; Wang, Y. Removal of Sulfadiazine from Aqueous Solution on Kaolinite. *Front. Environ. Sci. Eng.* 2013, 7(6), 836–843. DOI: [10.1007/s11783-013-0513-4](https://doi.org/10.1007/s11783-013-0513-4).
- [32] Meng, Q.; Zhang, Y.; Meng, D.; Liu, X.; Zhang, Z.; Gao, P.; Lin, A.; Hou, L. Removal of Sulfadiazine from Aqueous Solution by in-situ Activated Biochar Derived from Cotton Shell. *Environ. Res.* 2020, 191, 110104. DOI: [10.1016/j.envres.2020.110104](https://doi.org/10.1016/j.envres.2020.110104).
- [33] Eniola, J. O.; Kumar, R.; Barakat, M. A. Adsorptive Removal of Antibiotics from Water over Natural and Modified Adsorbents. *Environ. Sci. Pollut. Res.* 2019, 26(34), 34775–34788. DOI: [10.1007/s11356-019-06641-6](https://doi.org/10.1007/s11356-019-06641-6).
- [34] Livani, M. J.; Ghorbani, M. Fabrication of NiFe<sub>2</sub>O<sub>4</sub> Magnetic Nanoparticles Loaded on Activated Carbon as Novel Nanoadsorbent for Direct Red 31 and Direct Blue 78 Adsorption. *Environ. Technol. (United Kingdom)*. 2018, 39, 2977–2993.
- [35] Mahmoodi, N. M.; Salehi, R.; Arami, M. Binary System Dye Removal from Colored Textile Wastewater Using Activated Carbon: Kinetic and Isotherm Studies. *Desalination*. 2011, 272(1–3), 187–195. DOI: [10.1016/j.desal.2011.01.023](https://doi.org/10.1016/j.desal.2011.01.023).
- [36] Homem, V.; Alves, A.; Santos, L. Amoxicillin Removal from Aqueous Matrices by Sorption with Almond Shell ashes. *Int. J. Environ. Anal. Chem.* 2010, 90(14–15), 1063–1084. DOI: [10.1080/03067310903410964](https://doi.org/10.1080/03067310903410964).
- [37] Munagapati, V. S.; Kim, D. S. Equilibrium Isotherms, Kinetics, and Thermodynamics Studies for Congo Red Adsorption Using Calcium Alginate Beads Impregnated with nano-goethite. *Ecotoxicol. Environ. Saf.* 2017, 141, 226–234. DOI: [10.1016/j.ecoenv.2017.03.036](https://doi.org/10.1016/j.ecoenv.2017.03.036).
- [38] Priyantha, N.; Lim, L.; Dahri, M. K.; Lim, L.; B, L. Dragon Fruit Skin as a Potential Low-Cost Biosorbent for the Removal of Manganese(II) Ions. *J. Appl. Sci. Environ. Sanit.* 2013, 8, 179–188.
- [39] Zhang, X.; Zhang, Y.; Ngo, H. H.; Guo, W.; Wen, H.; Zhang, D.; Li, C.; Qi, L. Characterization and Sulfonamide Antibiotics Adsorption Capacity of Spent Coffee Grounds Based Biochar and Hydrochar. *Sci. Total Environ.* 2020, 716, 137015. DOI: [10.1016/j.scitotenv.2020.137015](https://doi.org/10.1016/j.scitotenv.2020.137015).
- [40] Wang, Y.; Jiao, W. B.; Wang, J. T.; Liu, G. F.; Cao, H. L.; Lü, J. Amino-functionalized biomass-derived Porous Carbons with Enhanced Aqueous Adsorption Affinity and Sensitivity of Sulfonamide Antibiotics. *Bioresour. Technol.* 2019, 277, 128–135. DOI: [10.1016/j.biortech.2019.01.033](https://doi.org/10.1016/j.biortech.2019.01.033).
- [41] Liu, Y.; Peng, Y.; An, B.; Li, L.; Liu, Y. Effect of Molecular Structure on the Adsorption Affinity of Sulfonamides onto CNTs: Batch Experiments and DFT Calculations. *Chemosphere*. 2020, 246, 125778. DOI: [10.1016/j.chemosphere.2019.125778](https://doi.org/10.1016/j.chemosphere.2019.125778).
- [42] Kazemi, E.; Dadfarnia, S.; Haji Shabani, A. M. Synthesis of a Novel Molecularly Imprinted Polymer Based on Functionalized multi-walled Carbon Nanotubes for Selective Extraction of Sulfadiazine Prior to Spectrophotometric Determination. *J. Iran. Chem. Soc.* 2017, 14(9), 1935–1944. DOI: [10.1007/s13738-017-1132-y](https://doi.org/10.1007/s13738-017-1132-y).
- [43] Wang, B.; Xu, X.; Tang, H.; Mao, Y.; Chen, H.; Ji, F. Highly Efficient Adsorption of Three Antibiotics from Aqueous Solutions Using glucose-based Mesoporous Carbon. *Appl. Surf. Sci.* 2020, 528, 147048. DOI: [10.1016/j.apsusc.2020.147048](https://doi.org/10.1016/j.apsusc.2020.147048).
- [44] Zuo, X.; Qian, C.; Ma, S.; Xiong, J. Sulfonamide Antibiotics Sorption by High Silica ZSM-5: Effect of pH and Humic Monomers (Vanillin and Caffeic Acid). *Chemosphere*. 2020, 248, 126061. DOI: [10.1016/j.chemosphere.2020.126061](https://doi.org/10.1016/j.chemosphere.2020.126061).
- [45] Gkotsis, P.; Peleka, E.; Zouboulis, A. The Use of Natural Minerals in a pilot-scale MBR for Membrane Fouling Mitigation. *Separations*. 2020, 7(2), 1–13. DOI: [10.3390/separations7020024](https://doi.org/10.3390/separations7020024).
- [46] Bracklow, U.; Drews, A.; Vocks, M.; Kraume, M. Comparison of Nutrients Degradation in Small Scale Membrane Bioreactors Fed with synthetic/domestic Wastewater. *J. Hazard. Mater.* 2007, 144(3), 620–626. DOI: [10.1016/j.jhazmat.2007.01.085](https://doi.org/10.1016/j.jhazmat.2007.01.085).
- [47] Kataria, N.; Garg, V. K. Green Synthesis of Fe<sub>3</sub>O<sub>4</sub> Nanoparticles Loaded Sawdust Carbon for Cadmium (II) Removal from Water: Regeneration and Mechanism. *Chemosphere*. 2018, 208, 818–828. DOI: [10.1016/j.chemosphere.2018.06.022](https://doi.org/10.1016/j.chemosphere.2018.06.022).